In Situ Synthesis of Polymer Nanocomposite Electrolytes Emitting a High Luminescence with a Tunable Wavelength

ARTICLE *in* THE JOURNAL OF PHYSICAL CHEMISTRY B · FEBRUARY 2003

Impact Factor: 3.3 · DOI: 10.1021/jp022223c

3 AUTHORS, INCLUDING:

Mikrajuddin Abdullah
Bandung Institute of Technology
129 PUBLICATIONS **714** CITATIONS
SEE PROFILE

Wuled Lenggoro
Tokyo University of Agriculture and Technology
122 PUBLICATIONS **3,226** CITATIONS
SEE PROFILE

In Situ Synthesis of Polymer Nanocomposite Electrolytes Emitting a High Luminescence with a Tunable Wavelength

Mikrajuddin Abdullah, I. Wuled Lenggoro, and Kikuo Okuyama*

Division of Chemistry and Chemical Engineering, Graduate School of Engineering, Hiroshima University, Higashi, Hiroshima 739-8527, Japan

Frank G. Shi

Department of Chemical Engineering & Materials Science, University of California, Irvine, California 92697-2575

Received: October 14, 2002

Zinc oxide (ZnO) nanoparticle-based nanocomposite polymer electrolytes with a very high luminescence intensity were prepared by an in situ method, in which ZnO nanoparticle fillers were grown in the polymer matrix and ion carriers were inserted during the growth of the nanoparticles (contributed by a precursor). By using a high concentration of lithium hydroxide (LiOH) as the precursor, the remaining unreacted LiOH was distributed in the form of an amorphous complex around the produced ZnO nanoparticles, thus preventing the agglomeration of the nanoparticles. This resulted in a high number concentration of ZnO nanoparticles that serve as luminescent centers for inducing a high luminescence intensity. Compared to samples prepared using the usual concentration of LiOH (about 0.14 M), the luminescence intensity was enhanced by about 22 times for the ZnO nanopowder and 6 times for the nanocomposite polymer electrolytes (poly(ethylene glycol)/ZnO/Li^+) when a LiOH concentration of 0.35 M was used.

Introduction

ZnO is a semiconductor material that produces an efficient blue-green luminescence. It serves as an efficient material for use in low-voltage phosphors and vacuum fluorescent displays as well as field emission displays (FEDs).[1] Recently, the last application has become even more important because FEDs are one of the promising candidates for use in next generation flat panel displays.[2] The discovery of a quantum size effect in nanometer sized particles, such as a dependence of optical spectrum on particle size has led to even more interest in ZnO materials.

In a previous report we described an in-situ method for preparing nanocomposite polymer electrolytes.[3] ZnO nanoparticles were grown directly in the polymer matrix and precursor materials containing alkali ions, which did not participate in the formation of nanoparticles were used.[3] Because ZnO nanoparticles emit luminescence, luminescent polymer electrolytes nanocomposites in which the nanoparticles serve as luminescent centers could be produced.[3] The measured electrical conductivity was found to be comparable with the data for composites made by dispersing preprepared particles in polymer/salt solutions.[4,5]

The luminescence intensities of the resulting composites, however, were still too weak,[3] especially when compared with rare earth based luminescent materials.[6,7] We attempted to use high concentrations of LiOH in the production of ZnO-based polymer electrolyte nanocomposites on the expectation that the excess LiOH woul served as a separator for the nanoparticles so that small sized, nonagglomerated, and high number concentration ZnO nanoparticles could be produced, generating a strong luminescence intensity. In the first part we focused on the production of ZnO nanopowder (dried colloid) and in the second we applied that approach to the production of ZnO-based polymer electrolyte nanocomposites.

Experimental Section

In principle, the preparation method was similar to that reported previously.[3] A solution of zinc acetate dihydrate ($Zn(CH_3COO)_2 \cdot 2H_2O$) in ethanol was distilled at 80 °C to produce 40 vol % of a hygroscopic solution and 60 vol % of unused condensate.[8] The lithium hydroxide hydrate ($LiOH \cdot H_2O$) was dissolved in ethanol separately and then mixed with the hygroscopic solution of zinc acetate ($Zn(CH_3COO)_2$/LiOH = 2/3 v/v). The concentrations of the lithium hydroxide used were typically less than 0.14 M.[8,9] An extensive mixing process was required even to dissolve lithium hydroxide at concentrations below 0.14 M. A highly concentrated lithium hydroxide solution was prepared here by dissolving the lithium hydroxide in ethanol with stirring for around 3 h at elevated temperatures (around 50 °C). Several minutes after mixing the precursors, the mixture was then dried at 40 °C for about 3 days to produce a ZnO nanopowder. We used three concentrations of LiOH to produce ZnO nanopowders: (i) 0.075 M, (ii) 0.14 M, and (iii) 0.35 M. On the other hand, to prepare polymer electrolyte nanocomposites, we used LiOH concentrations of (i) 0.05 M, (ii) 0.075 M, (iii) 0.1 M, (iv) 0.14 M, (v) 0.2 M, (vi) 0.25 M, (vii) 0.3 M, (viii) 0.35 M, and (ix) 0.5 M. Poly(ethylene glycol) (PEG) 500 000 (0.5 g) was dissolved in the lithium hydroxide solution at a temperature of approximately 50 °C before mixing with the zinc acetate precursor. The mixture was then dried at 40 °C for 3 days.

X-ray diffraction patterns were obtained using a Rigaku Denki RINT2000 instrument (Cu Kα source), electrical conductivities

* Corresponding author. E-mail: okuyama@hiroshima-u.ac.jp.

10.1021/jp022223c CCC: $25.00
Published on Web 02/07/2003

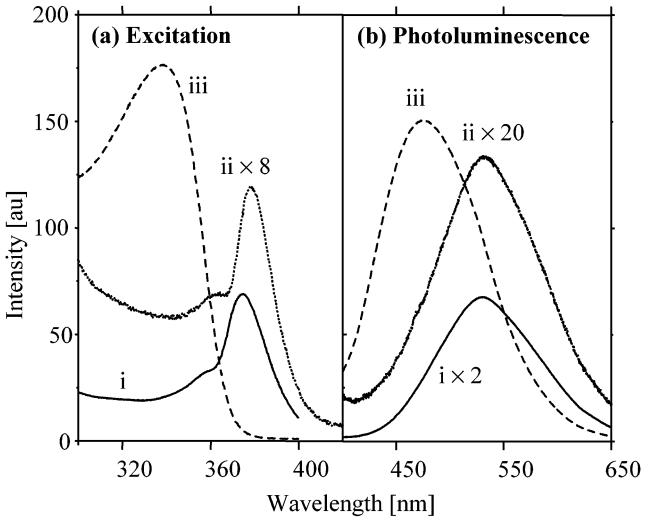

Figure 1. (a) Excitation spectra and (b) photoluminescence spectra of ZnO nanopowder samples i−iii. The excitation spectra were detected at $\lambda = 533$ nm, whereas the photoluminescence spectra were excited at wavelengths equal to the highest peaks in the excitation spectra.

were measured using a Precision LCR Meter Agilent HP4284A (1 kHz), excitation and luminescence spectra were measured using a Shimazu RF-5300PC (Xe source) at room temperature, and transmission electron micrograph (TEM) images were recorded using a Hitachi H-7000FA (100 kV) instrument at the Toray Research Center (Shiga, Japan).

Results and Discussion

ZnO Nanopowder. Figure 1a shows the excitation spectra of ZnO nanopowder samples i−iii detected at 533 nm in a reflection mode. The samples were pressed in an aluminum cap, and spectra were automatically obtained using the RF-5300PC photometer when detected at a certain wavelength. The intensity first decreased for samples i and ii and then increased by about 12 times for sample iii. Sample i showed a weak peak at 358 nm and a strong peak at 374 nm, whereas sample ii showed a weak peak at 361 nm and a strong peak at 379 nm.

The short-wavelength peak, which is shorter than the band gap wavelength of the bulk ZnO (around 365 nm), is related to the transition of electrons from the top of the valence band to the bottom of the conduction band (band gap peak). On the other hand, the long-wavelength peak should correspond to an electron transition from the top of the valence band to the exciton levels (exciton peak). The difference in the energies of the band gap peak and the exciton peak were determined to be around 90 meV. The theoretical value of the exciton energy (quantum number $\boldsymbol{n} = 1$), measured from the bottom of the conduction band is given by $E_{ex} = (\mu/m_e\kappa^2) \times 13.6$ eV,[10] with $1/\mu = 1/m^*_e + 1/m^*_h$, where m^*_e and m^*_h are the effective masses of electron and hole, respectively and κ is the dielectric constant of ZnO. Introducing $m^*_e = 0.31m_e$, $m^*_h = 0.8m_e$, with m_e as the free mass of an electron and $\kappa = 6$ as predicted by Enright and Fitzmaurice,[11] we obtained $E_{ex} = 82$ meV, in reasonable agreement with our experimental observation.

An exciton peak was not observed for the ZnO colloid. Only the band gap peak with a wavelength shorter than 365 nm was found.[8] Therefore, we assume that the presence of the exciton peak is related to the presence of a higher number density ZnO nanoparticles, and possibly, to agglomeration. The excitation spectra composite produced by spray drying of a ZnO colloid and a colloid of silica nanoparticles can be found in our previous report[12] and was also consistent with the results reported here. The exciton peaks decreased consistently when the weight fraction of SiO_2 increased relative to ZnO. This increase is indicative of a favorable separation of the ZnO nanoparticles in the composite. A ZnO film prepared on a glass substrate by spray pyrolysis as reported by Studenikin et al.[13] also showed the presence of an exciton peak with a wavelength peak at around 370 nm. The ZnO nanocrystals were connected to each other to form strong film; i.e., their morphology was similar to that of agglomerated nanocrystals.

The shape of the excitation spectra of sample iii is significantly different from those of samples i and ii. No exciton peak was observed in this sample, similar to that observed for a ZnO colloid.[10] This suggests that ZnO nanoparticles in the sample iii were separated from each other. Because a large amount of lithium hydroxide was used, a fraction of lithium hydroxide must be left in the sample. The excess lithium hydroxide used in the precursor served as a separator for the ZnO nanoparticles that were produced. This suggestion was similar to the result reported by Xia et al. on producing oxide nanoparticles via an aerosol decomposition (spray pyrolysis) method by adding a eutectic mixture of a simple salt ($LiNO_3$, $NaNO_3$, etc.) to the precursor solution.[14] During the drying process, the salt served as separator for nanoparticles, thus preventing agglomeration.

Figure 1b shows photoluminescence spectra of samples i to iii excited using a wavelength that coincided with the highest peak in the excitation spectra. Sample ii, produced using a commonly used lithium hydroxide concentration,[8] exhibited a very weak photoluminescence intensity. Sample iii exhibited a very high photoluminescence intensity, i.e., about 22 times larger than that of sample ii. This large enhancement in intensity was achieved due to the fact that the number particle concentration of ZnO nanoparticles in sample iii was much higher than in others because of their smaller size. This was also supported by the location of photoluminescence peak of sample iii, which is to the left of those of samples i and ii, to indicate a reduction in particle size.

Using the above wavelengths for the excitation source, the emission at about 380 nm was not observed. This low intensity emission could be observed when a shorter excitation wavelength (around 250 nm) was used.

We estimated the average size of the ZnO nanoparticles using a well-known formula $E_g(r) = E_g^\infty + h^2/8\mu R^2 - 1.8\ e^2/4\pi\epsilon_o\kappa R$, where R is the nanocrystallite radius, E_g^∞ is the band gap of a bulk crystal of ZnO, and h is Planck's constant.[1] The band gap of bulk ZnO is $E_g^\infty = 3.4$ eV. Using the position of the excitation peaks at 358, 361, and 339 nm for ZnO nanopowders samples i−iii, respectively, it was possibly to obtain a rough approximation of the average diameter of the ZnO nanocrystals in samples i−iii of 7.2, 8.6, and 4.3 nm, respectively. Our estimation was compared with the TEM image of sample ii. A small amount of nanopowder was dispersed in ethanol and placed in an ultrasonic bath for about 30 min. A droplet of the resulting mixture was placed on a TEM grid (carbon) and dried at room temperature. As shown in Figure 2a, the average size of the ZnO nanoparticles in this sample was around 7−8 nm, very close to our prediction (8.6 nm). We were unable to obtain a clear picture of sample iii, because the size of the ZnO nanoparticles are much smaller.

Polyethylene Glycol/ZnO Nanoparticles Composites. We also attempted to use PEG with molecular weights of 2×10^4, 2×10^6, and 4×10^6, but the properties of the composite produced using PEG 500 000 exceeded the others on the basis of the film morphology and repeatibility. Figure 3a shows the

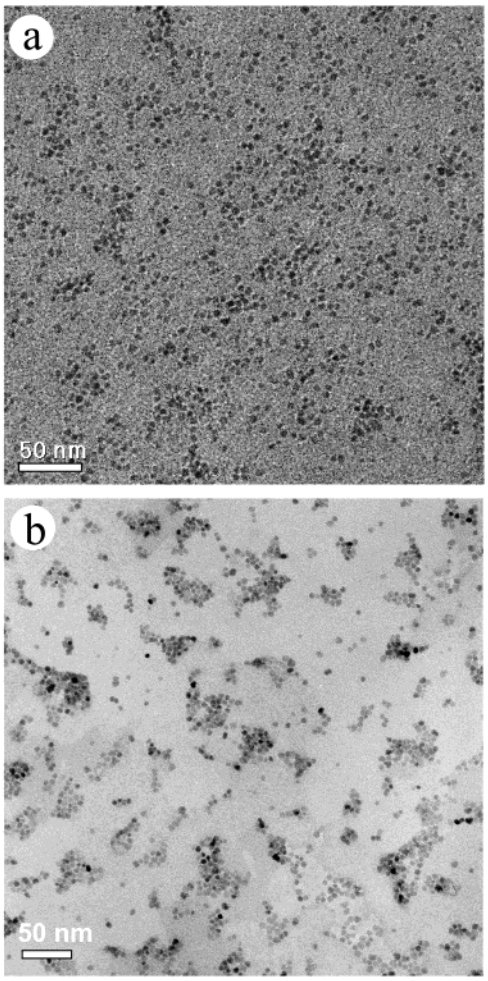

Figure 2. TEM image of (a) ZnO nanopowder sample (ii) (b) PEG/ZnO nanocomposites sample v.

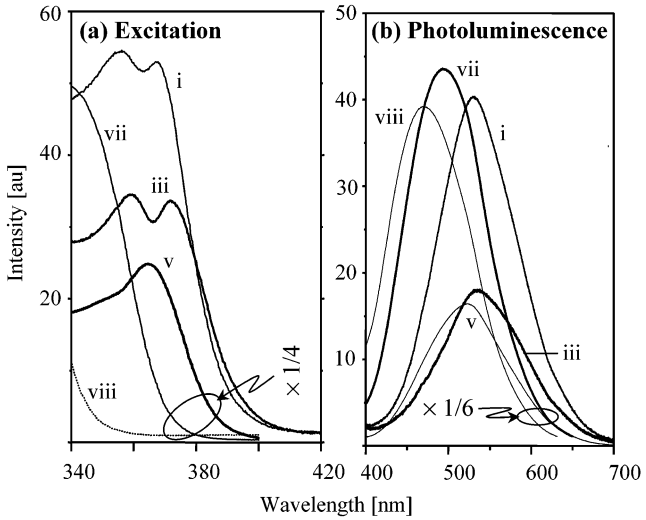

Figure 3. (a) Excitation spectra and (b) photoluminescence spectra of nanocomposite polymer electrolyte samples i, iii, v, vii, and viii. The excitation spectra were detected at $\lambda = 533$ nm, whereas the photoluminescence spectra were excited at wavelengths equal to the highest peaks in the excitation spectra.

excitation spectra of samples i, iii, v, vii, and viii detected at a wavelength of 533 nm. The band gap and exciton peaks in samples prepared using lithium hydroxide concentrations of less than 0.25 M were similar to that observed in samples i and ii of the ZnO nanopowder.

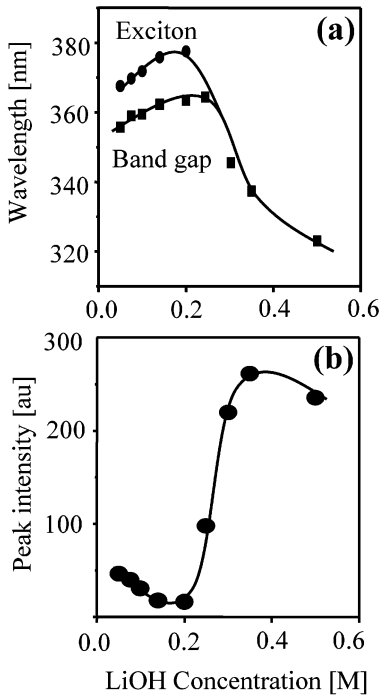

Figure 4. Effect of LiOH concentration on (a) the peak position of band gap excitation and exciton excitation and (b) photoluminescence intensity of the ZnO nanoparticles in PEG/ZnO composites samples.

On the other hand, a different shape for the excitation spectra in samples prepared using lithium hydroxide concentrations of larger than 0.2 M was found. The exciton peaks were absent in these cases. Only band gap transitions were observed, and their energies were much higher than those for samples prepared using a low concentration of lithium hydroxide. Thus, there was a turning point for ZnO nanoparticle size when the lithium hydroxide concentration was varied. Increasing the lithium hydroxide concentration first increased and then decreased the particle size, having reached a maximum size at a lithium hydroxide concentration of 0.25 M. Figure 4a shows the variation in the peak positions versus lithium hydroxide concentration, for exciton transition (circles) and band gap transition (squares). The peak positions changed abruptly for lithium hydroxide concentrations larger than 0.25 M.

As observed in the ZnO nanopowder, the disappearance of the exciton peak could have been caused by the presence of a lithium-rich compound surrounding the ZnO nanoparticles that served as a separator for the grown nanoparticles at the initial stage of growth. This state reduced both the tendency of small particles to agglomerate and continue to grow. The resulting particles were smaller in size and well distributed in the polymer matrix and consequently resulted in a drastic enhancement in the excitation peak by a factor of 400%.

Figure 3b shows the photoluminescence spectra of samples i, iii, v, vii, and viii. Excitation was achieved using wavelengths that coincided with the highest peaks in the excitation spectra. The position of the luminescence peak initially shifted to lower energies and then returned to higher energies when the LiOH concentration was larger than 0.25 M. As observed in Figure 4b, the intensity increased suddenly (percolation likely) when the LiOH concentration exceeded 0.2 M. The enhancement in luminescence intensity of around 600% was observed for samples prepared using LiOH concentrations of 0.35 and 0.5 M. This enhancement was a result of the increase in the number concentration of ZnO nanoparticles. The shift in the peak to higher energy was due to a decrease in particle size.

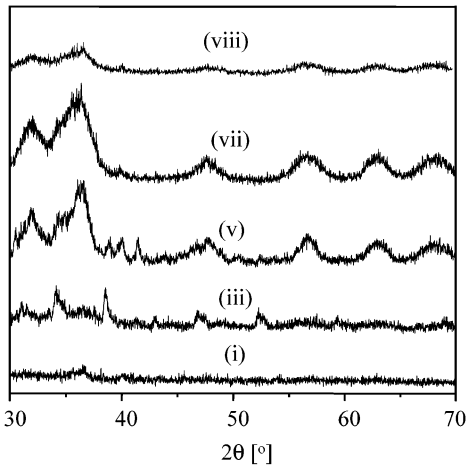

Figure 5. XRD patterns of PEG/ZnO nanocomposites i, iii, v, vii, and viii.

Similarly, we predicted the average particle size of ZnO nanoparticles in nanocomposite polymer electrolytes. The size initially increased with lithium hydroxide concentration, reaching a maximum value of around 11 nm for a lithium hydroxide concentration of 0.25 M. Interestingly, a further increase in the lithium hydroxide concentration reduced the crystalline size to about 5 nm for a lithium hydroxide concentration of 0.5 M. To confirm this prediction, we compared the calculated size and the TEM image of a sample prepared using a lithium hydroxide concentration of 0.14 M. Figure 2b shows the TEM image of a sample prepared using a lithium hydroxide concentration of 0.14 M. The average ZnO particles size is about 5 nm. Electron probe microanalysis was carried out to prove that the observed image was, in fact, ZnO nanoparticles. We also predicted that the particle size in this sample would be about 8.6 nm.

Figure 5 shows the XRD patterns of samples i, iii, v, vii, and viii. The intensity peaks increased with lithium hydroxide concentration, indicating an increase in the amount of ZnO nanoparticles in the matrix. The XRD pattern intensity reached a maximum value for a lithium hydroxide concentration of 0.25 M. A further increase in lithium hydroxide concentration to above 0.25 M reduced the XRD intensity, indicating that the ZnO nanoparticles were surrounded by amorphous material (unreacted lithium hydroxide) due to the use of excess lithium hydroxide in the precursor.

A correlation between the excitation spectra and XRD patterns was found. The XRD intensity increased when the lithium hydroxide concentration was increased up to 0.25 M and then decreased with a further increase to above 0.25 M. This is also the value when the exciton peak disappeared. The band gap energy that initially decreased by the increase in the lithium hydroxide concentration also began to decrease for lithium hydroxide concentrations larger than 0.25 M. A concentration of 0.25 M is roughly the saturation point for the lithium hydroxide concentration, above which all zinc ions had reacted. When the lithium hydroxide concentration was increased above 0.25 M, a definite portion of the lithium hydroxide reacted with zinc acetate and the remainder appeared to be a lithium complex. Therefore no further change in the amount of ZnO would be expected.

Figure 6a shows the temperature dependent electrical conductivity of samples ii−vi, measured in a nitrogen atmosphere. The samples were previously heated to the polymer melting point. We predicted that the melting point of high molecular weight PEG would be between 61 and 65 °C.[3] The conductivities were measured during the cooling cycle. For low lithium

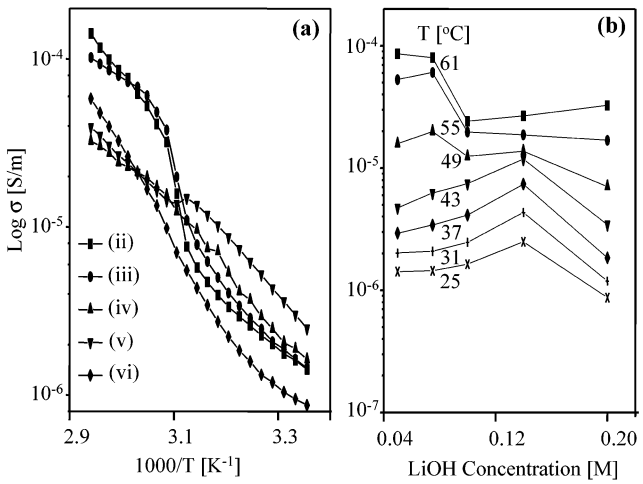

Figure 6. (a) Effect of temperature on the electrical conductivity of PEG/ZnO nanocomposite samples ii−vi, and (b) the dependence of electrical conductivities of PEG/ZnO nanocomposite samples as a function of LiOH concentrations at various temperatures.

hydroxide concentrations, the variation in conductivity could be described by the Vogel−Tamman−Fulcher principle at high temperatures and the Arrhenius relationship at low temperatures. For high lithium hydroxide concentrations, the conductivity obeyed the Arrhenius relationship in all temperature regions. It is also interesting to note that at high temperatures, the conductivity tended to decrease with increasing concentrations of lithium hydroxide and at low temperatures, the conductivity first increased and then decreased with increasing concentrations of lithium hydroxide, as shown in Figure 6b. A theoretical explanation of this conductivity variation is provided in appendix.

Conclusion

In summary, we were able to produce strong luminescent polymer electrolyte nanocomposites by an in situ process, both by the growth of nanoparticles and by the insertion of ion carriers into the polymer matrix. This method is facilitated by the selection of precursors containing ion carriers in which these ions do not participate in the formation of nanoparticles. Enhancements in excitation intensity of 400% and in luminescence intensity of 600% were found when high concentrations of lithium hydroxide precursor were used. It is assumed that this material produced a salt compound during the growth process, which becomes distributed on the surface of the nanoparticles, thus preventing them from agglomerating.

Acknowledgment. We thank Prof. Shuji Sakohara for valuable advice, Mr. Kazuhiko Tanaka for his assistant in experiments, and Mr. Tsutomu Morimoto for TEM measurement in the Toray Research Center. A postdoctoral fellowship from the Japan Society for the Promotion of Science for M.A. is gratefully acknowledged. A Grant-in-Aid for Exploratory Research (K.O., I.W.L.) and a Grant-in-Aid for Encouragement of Young Scientists sponsored by the Ministry of Education, Culture, Sports, Science, and Technology of Japan and the Japan Society for the Promotion of Science are gratefully acknowledged. This work was also supported by the New Energy and Industrial Technology Development Organization (NEDO)'s "Nanotechnology Materials Program - Nanotechnology Particle Project" based on funds provided by the Ministry of Economy, Trade, and Industry (METI), Japan.

Appendix

The conductivity variation in Figure 6b is interesting. Here, we attempted to use a modified effective medium approximation to explain the conductivity variation of the composites appearing in Figure 6b.[15] The presence of particles in the polymer electrolyte induced the presence of amorphous regions around the particles, leading to the development of a high conductivity layer at the interface between the particles and the electrolyte. We refer to this region as a high conductive region. At low temperatures, regions located far from the particle were in a crystalline state such that the conductivity was lower than that at the interface region. We refer to this region as a medium conductive region. When two particles made contact, the electrolyte medium between those particles is removed and the transport of ions did not take place. The conductivity of this region was reduced to close to zero (approximately equal to that of the insulator particles), and we refer to this as a low conductive region. The overall system could then be modeled as a three conductivities system. The conductivity development can be written as[15]

$$P_{\mathrm{l}}\frac{\sigma_{\mathrm{l}}-\sigma_{\mathrm{e}}}{\sigma_{\mathrm{l}}+(z/2-1)\sigma_{\mathrm{e}}}+P_{\mathrm{m}}\frac{\sigma_{\mathrm{m}}-\sigma_{\mathrm{e}}}{\sigma_{\mathrm{m}}+(z/2-1)\sigma_{\mathrm{e}}}+P_{\mathrm{h}}\frac{\sigma_{\mathrm{h}}-\sigma_{\mathrm{e}}}{\sigma_{\mathrm{h}}+(z/2-1)\sigma_{\mathrm{e}}}=0 \quad (1)$$

where σ_{l}, σ_{m}, and σ_{h} are the conductivities of low, medium, and high conductivity regions, respectively, σ_{e} is the effective conductivity of the composite, z is the coordination number, and P_{l}, P_{m}, and P_{h} are the probabilities of the existence of low, medium, and high conductive regions respectively, given by

$$P_{\mathrm{l}}=\frac{v^2}{f^2} \qquad P_{\mathrm{m}}\left(1-\frac{v}{f}\right)^2 \qquad P_{\mathrm{h}}=2\left(\frac{v}{f}\right)\left(1-\frac{v}{f}\right) \quad (2)$$

where f is the packing fraction and v the volume fraction of the particles.

We simulated the conductivity variation at various particle volume fractions to show that the proposed model is able to produce similar trend of conductivity variations. For simplicity we used a simple cubic packing of particles such that $z = 6$ and $f = \pi/6$. The three conductivities were set to satisfy $\sigma_{\mathrm{l}}/\sigma_{\mathrm{h}} = 0.02$ and $\sigma_{\mathrm{m}}/\sigma_{\mathrm{h}} = 0.1$. Curve a in Figure 7 shows the variation in conductivity at low temperatures. A bell shaped conductivity curve is seen as the volume fraction of particles increases. At a zero volume fraction of the particles, the conductivity of the composites is equal to that of the polymer in the crystalline phase. A fraction of particles exists such that the conductivity reaches a maximum value, and a threshold volume fraction of particles exists such that the conductivity tends toward zero. A similar shape was observed in various composites of insulating particles and a solid-state ionics matrix.[16−19]

At high temperatures, on the other hand, not only the regions around the particle surface were amorphous. Nearly all parts of the polymer existed in amorphous states. Therefore, the conductivity of the high and medium conductivity regions became similar, or $\sigma_{\mathrm{m}} = \sigma_{\mathrm{h}}$. Using this value and maintaining $\sigma_{\mathrm{l}}/\sigma_{\mathrm{h}} = 0.02$, curve b in Figure 7 is obtained. The presence of nanoparticles simply blocks the transfer of ion carriers. The conductivity always decreases with an increase in the volume fraction of the particles. A similar phenomenon has been observed by Furusawa et al in solid-state ionic composites.[20]

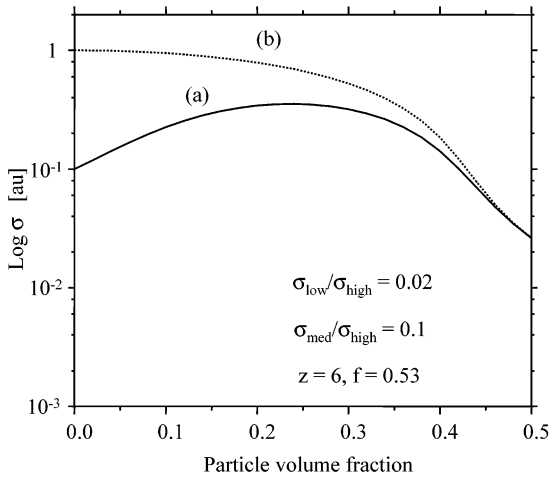

Figure 7. Calculated variation in electrical conductivities with respect to the volume fraction of nanoparticles at (a) low temperatures and (b) high temperatures.

In our nanocomposites, the use of high concentrations of lithium hydroxide was equivalent to the use of a large volume fraction of ZnO nanoparticles. Our prediction, therefore, qualitatively, could produce the trend obtained by experiment. At the present time, we were not be able to directly test our theoretical prediction with the experimental data because the dependence of the produced ZnO nanoparticles on the concentration of lithium hydroxide is not known. Further studies will be required to determine this relationship.

References and Notes

(1) van Dijken, A.; Meulenkamp, E. A.; Vanmaekelbergh, D.; Meijerink, A. *J. Lumin.* **2000**, *90*, 123.
(2) Shionoya, S.; Yen, W. M., Eds. *Phosphor Handbook*, CRC Press: Boca Raton, FL, 2000; p 255.
(3) Mikrajuddin; Lenggoro, I. W.; Okuyama, K.; Shi, F. G. *J. Electrochem. Soc.* **2002**, *149*, H107.
(4) Croce, F.; Appetecchi, G. B.; Persi, L.; Scrosati, B. *Nature* **1998**, *394*, 456.
(5) Kumar, B.; Scanlon, L. G. *J. Electroceramics* **2000**, *52*, 127.
(6) Kang, Y. C.; Lenggoro, I. W.; Park, S. B.; Okuyama, K. *Appl. Phys. A* **2001**, *72*, 103.
(7) Kang, Y. C.; Park, S. B.; Lenggoro, I. W.; Okuyama, K. *J. Mater. Res.* **1999**, *14*, 2611.
(8) Spanhel, L.; Anderson, M. A. *J. Am. Chem. Soc.* **1991**, *113*, 2826.
(9) Sakohara, S.; Ishida, M.; Anderson, M. A. *J. Phys. Chem. B* **1998**, *102*, 10169.
(10) Yu, P. Y.; Cardona, M. *Fundamentals of Semiconductors*; Springer-Verlag: Berlin/Heidelberg, 1996; p 272.
(11) Enright, B.; Fitzmaurice, D. *J. Phys. Chem.* **1996**, *100*, 1027.
(12) Mikrajuddin; Iskandar, F.; Shi, F. G.; Okuyama, K. *J. Appl. Phys.* **2001**, *89*, 6431.
(13) Studenikin, S. A.; Golego, N.; Cocivera, M. *J. Appl. Phys.* **1998**, *84*, 2287.
(14) Xia, B.; Lenggoro, I. W.; Okuyama, K. *Adv. Mater.* **2001**, *13*, 1579.
(15) Mikrajuddin; Shi, F. G.; Okuyama, K. *J. Electrochem. Soc.* **2000**, *147*, 3157.
(16) Liang, C. J. *J. Electrochem. Soc.* **1973**, *120*, 1289.
(17) Jow, T.; Wagner, J. B. *J. Electrochem. Soc.*, **1979**, *126*, 1963.
(18) Kumar, B.; Scanlon, L. G. *J. Power Sources* **1994**, *52*, 261.
(19) Przylusky, P.; Siekiersk, M.; Wieczore, W. *Electrochim. Acta* **1995**, *40*, 2102.
(20) Furusawa, S.; Miyaoka, S.; Ishibashi, Y. *J. Phys. Soc. Jpn.* **1991**, *60*, 1666.